QCD phase transition at finite temperature and chemical potential with nonextensive statistics

Zhi-Ying Qin,[1,2] Jia-Hao Shi,[1,3] Jin-Peng Zhang,[1] Jian Cao,[1] Bo Feng,[1] Wen-Chao Zhang,[1,*] Hua Zheng,[1] and Shi-Jun Mao[4]

[1]*School of Physics and Information Technology, Shaanxi Normal University, Xi'an 710119, China*
[2]*School of Physics Science and Engineering, Tongji University, Shanghai 200092, China*
[3]*Key Laboratory of Quark and Lepton Physics (MOE) and Institute of Particle Physics, Central China Normal University, Wuhan 430079, China*
[4]*School of Physics, Xi'an Jiaotong University, Xi'an, Shaanxi 710049, China*

(Received 1 July 2025; revised 24 September 2025; accepted 7 October 2025; published 19 November 2025)

The intrinsic fluctuations, memory effects, and long-range color interactions in high-energy nuclear collisions imply the presence of non-Markovian processes in the fireball evolution, which affects the thermalization process toward equilibrium and produces a nonextensive behavior. In order to investigate the nonequilibrium effect on the quantum chromodynamics (QCD) phase transition at finite temperature (T) and chemical potential (μ), we apply a nonextensive correction to the equation of state in the parton (hadron resonance) gas at high (low) temperature and interpolate these two equations of state with a smooth crossover. The nonextensive statistics is characterized by a nonextensivity parameter q, which measures the degrees of deviation from the thermal equilibrium. It is found that the dimensionless thermodynamic quantities such as the entropy density, the pressure, the energy density, the specific heat at constant volume, and the trace anomaly are sensitive to the deviation of q from unity, and they become large in both the hadronic and quark-gluon plasma phases with the increase of q. Moreover, this deviation leads to nontrivial corrections of the squared speed of sound $[(c_s^2)_q]$ in the vicinity of the critical point (T_c) and at lower temperatures. Additionally, these thermodynamic quantities are sensitive to the deviation of μ from zero. With increasing μ, they become enhanced in both phases. Specifically, for $(c_s^2)_q$, the value increases near T_c but decreases at lower temperatures. Finally, we observe that our results with $q = 1$ agree well with those from lattice QCD, the hadron resonance gas model, and the Thermal-Fist fit to the hadron yields in high-energy nuclear collisions in the low-temperature region up to $T \sim 150$ MeV.

DOI: 10.1103/4gzt-46t5

I. INTRODUCTION

Quantum chromodynamics (QCD) predicts that at high temperatures and energy densities, there exists a deconfining transition of the matter governed by strong interactions to a new state, denoted as the quark-gluon plasma (QGP). QGP is expected to be produced in ultrarelativistic heavy-ion collisions. Exploring the properties of QCD phase transition is one of the main goals in heavy-ion collisions.

Several effective models, such as the bag model [1], the Nambu–Jona-Lasinio (NJL) model [2,3], the linear sigma model [4], the quark-meson model [5,6], the Dyson-Schwinger equations approach [7,8], the functional renormalization group approach [9–11], the hadron resonance gas (HRG) and statistical models [12–15], and lattice QCD (LQCD) [14–17], have been utilized to investigate the properties of the QCD phase transition. In these models, a thermal equilibrium is assumed, and an extensive statistical approach, such as Boltzmann-Gibbs (BG) statistics, Bose-Einstein statistics, or Fermi-Dirac statistics, is applied.

However, such an approach is only valid when the heat bath of the system is homogeneous. In reality, this condition cannot always be fulfilled. For example, in high-energy nucleus-nucleus (AA) collisions, extreme conditions of density and temperature give rise to strong intrinsic fluctuations, memory effects, and long-range correlations [18–21]. These conditions imply the presence of non-Markovian processes in the fireball evolution, which affects the thermalization process toward equilibrium and the standard equilibrium distribution [22]. Thus, instead of an equilibrium state, some kind of stationary state near the equilibrium (q-equilibrium) is expected to be formed

*Contact author: wenchao.zhang@snnu.edu.cn

[23,24]. This phenomenon can be dealt with nonextensive statistics (Tsallis statistics) [25], where the degree of deviation from the equilibrium is described by a single parameter q. The nonextensivity in a QCD system can also be understood as a result of the fractal structure of the hot and dense system formed in high-energy nuclear collisions [26,27].

In recent years, Tsallis statistics has been widely employed to describe the multiparticle production processes in high-energy proton-proton (pp) [28–36] and AA [37–45] collisions. In most of these applications, the Tsallis distribution or the Tsallis-extended blast wave model is simply fitted to the particle transverse momentum (p_{T}) spectra. The extracted values of q from the fits are usually larger than 1. The deviation of q from unity represents the intrinsic fluctuations of the temperature [18], or of the mean value of the charged-particle multiplicity [46] in the hadronizing system. This deviation can be also be related to the fractal dimension of the hadronizing system [26,27]. In the case of high-energy AA collisions, the fluid dynamics is not considered in these applications, which could affect the accuracy of the results. In light of such a situation, $(0+1)$-, $(1+1)$-, $(2+1)$-, and $(3+1)$-dimensional hydrodynamic models based on nonextensive statistics were developed as a description of relativistic heavy-ion collisions [20,47–49]. This is a reasonable extension of the hydrodynamic model, as far-from-equilibrium evolution can still obey the hydrodynamic equations of motion, provided that the system is locally isotropized in the comoving frame of the fluid [50,51]. It was shown that the nonextensive hydrodynamic model can describe the charged hadron p_{T} spectra up to 6–8 GeV$/c$, which is larger than the typical validity range of the extensive hydrodynamic description, 2–3 GeV$/c$. Moreover, the elliptic flow of charged particles was reduced with the introduction of Tsallis statistics to the hydrodynamic model. Tsallis statistics has also been applied on the nuclear equation of state (EOS) and the QGP EOS in the framework of a relativistic mean-field approach and the bag model, respectively. In the former model, the interactions of nucleons are mediated by the exchange of isoscalar and isovector mesons, σ, ω, and ρ [22,52–54]. In the latter model, the quark matter is described as a gas of free quarks, and the nonperturbative effects are simulated by the bag constant B [22,52,54]. It was observed that both the nuclear EOS and the QGP EOS became stiffer when the nonextensive statistic effect was considered. Furthermore, Tsallis statistics has been taken into account in the NJL model to describe the QCD phase transition [55–58]. It was found that with the increase of q, the critical end point moved toward the direction of larger chemical potential and lower temperature.

In this study, in order to investigate the nonextensive effect on the QCD phase transition at finite temperature and chemical potential, we apply a nonextensive correction to the EOS in the parton (hadron resonance) gas [13,59,60] at high (low) temperature and interpolate these two equations of state with a smooth crossover. We first explore the QCD phase transition with zero chemical potential. In the QGP phase, the dominant excitations are the massive u, d, and s quarks, while in the hadronic phase, they are the hadrons and resonances composed of u, d, and s quarks with masses below 2.5 GeV$/c^2$. Then, we investigate the QCD phase transition with finite chemical potential. We will investigate the effects of the nonextensive statistics as well as the chemical potential on the temperature dependence of the dimensionless thermodynamic quantities such as the entropy density, the pressure, the energy density, the trace anomaly, the heat capacity at constant volume, and the squared speed of sound. Moreover, we will compare our results with those from the HRG, the LQCD, and the fit of the experimental yields of hadrons at the LHC and RHIC energies using the Thermal-Fist package [61].

This paper is organized as follows: In Sec. II, we will describe the Tsallis statistics and construct a nonextensive version of the EOS by applying the nonextensive correction to the EOS in the parton (hadron resonance) gas at high (low) temperature and making a smooth interpolation of these two equations of state. In Sec. III, we will discuss the effects of the nonextensive statistics and the chemical potential on the thermodynamic quantities and compare our results with different models. Finally, the conclusion is given in Sec. IV.

II. THE MODEL

A. Tsallis statistics

This description of nonextensive statistics was first proposed by Tsallis [62]. It generalizes the BG statistics and defines the entropy of a system as

$$S_q = k\left(1 - \sum_{R=1}^{W} p_R^q\right) \Big/ (q-1), \tag{1}$$

where k is a positive constant; $W \in N$ is the total number of microscopic configurations of the system; p_R is the probability associated with the Rth state and satisfies $\sum_{R=1}^{W} p_R = 1$; and q characterizes the degree of nonextensivity reflected in the following pseudoadditive rule for a composite system consisting of two individual systems A and B:

$$\frac{S_q(A+B)}{k} = \frac{S_q(A)}{k} + \frac{S_q(B)}{k} + (1-q)\frac{S_q(A)}{k}\frac{S_q(B)}{k}. \tag{2}$$

In the limit $q \to 1$, the expression in Eq. (1) approaches the BG entropy,

$$\lim_{q\to 1} S_q = -k\sum_{R=1}^{W} p_R \ln p_R. \tag{3}$$

In order to determine the probability distribution of a state R in a grand-canonical system, we need to maximize the entropy under the internal energy and particle number constraints,

$$\bar{E} = \sum_{R=1}^{W} p_R^q E_R, \tag{4}$$

$$\bar{N} = \sum_{R=1}^{W} p_R^q N_R, \tag{5}$$

where $\bar{E}$ and $\bar{N}$ are, respectively, the average energy and the average number of particles. The maximization of the entropy under the constraints in Eqs. (4) and (5) leads to the variational equation

$$\frac{\delta}{\delta p_R}\left(\frac{S_q}{k} - \alpha\sum_{R=1}^{W} p_R - \beta\sum_{R=1}^{W} p_R^q E_R - \gamma\sum_{R=1}^{W} p_R^q N_R\right) = 0, \tag{6}$$

where α, β, and γ are the Lagrange multipliers associated with the total probability, the total energy, and the total number of particles, respectively. Following the standard thermodynamic definitions, such as $\beta = 1/T$ and $\gamma = -\beta\mu$ with T and μ being the temperature and the chemical potential of the system, respectively, the probability distribution of the state R in the grand-canonical ensemble is written as

$$p_R = [1 + (q-1)(E_R - \mu N_R)/T]^{1/(1-q)}/Z_q, \tag{7}$$

where

$$Z_q = \sum_R [1 + (q-1)(E_R - \mu N_R)/T]^{1/(1-q)} \tag{8}$$

is the partition function of the grand-canonical system.

The quantum state of the system is uniquely determined when occupation numbers of the one-particle states are provided. The total energy and the total particle numbers of the system in the state R are then automatically given by

$$E_R = n_1\varepsilon_1 + n_2\varepsilon_2 + \cdots + n_k\varepsilon_k + \cdots, \tag{9}$$

$$N_R = n_1 + n_2 + \cdots + n_k + \cdots, \tag{10}$$

where ε_k and n_k are, respectively, the energy of a particle and the number of particles in the state k. Substituting Eqs. (9) and (10) into Eq. (8), one gets the partition function as [63]

$$\begin{aligned} Z_q &= \sum_{n_1,n_2\cdots,n_k,\cdots} \exp_q\left(-\frac{(\varepsilon_1-\mu)n_1}{T}\right) \\ &\quad \otimes_q \exp_q\left(-\frac{(\varepsilon_2-\mu)n_2}{T}\right) \otimes_q \cdots \\ &\quad \otimes_q \exp_q\left(-\frac{(\varepsilon_k-\mu)n_k}{T}\right) \otimes_q \cdots \\ &= \left(\prod_{k=1}^{\infty}\right)_q \sum_{n_{k=0}}^{\infty} \exp_q\left(-\frac{(\varepsilon_k-\mu)n_k}{T}\right), \end{aligned} \tag{11}$$

where $\exp_q(x) = [1 + (1-q)x]^{(1/(1-q))}$, $\exp_q(x) \otimes_q \exp_q(y) = \exp_q(x+y)$, and $(\prod)_q$ means successive q-multiplication. When taking into account the d internal degrees of freedom for the noninteracting fermions and bosons, respectively, the grand-canonical partition function becomes

$$Z_q = \left(\prod_{k=1}^{\infty}\right)_q \left[1 + \exp_q\left(-\frac{\varepsilon_k-\mu}{T}\right)\right]^{+d} \tag{12}$$

and

$$Z_q \approx \left(\prod_{k=1}^{\infty}\right)_q \left[1 - \exp_q\left(-\frac{\varepsilon_k-\mu}{T}\right)\right]^{-d}. \tag{13}$$

The derivations of Eqs. (12) and (13) are shown in Appendix A. In the derivation of Eq. (13), we have made an approximation in which the higher orders $\mathcal{O}(q-1)^2$ have been ignored.

B. Equations of state in the hadronic and QGP phases

In the framework of extensive statistics, the grand-canonical potential Ω is related to the grand-canonical partition function Z as follows [64]:

$$\Omega = -T\ln Z. \tag{14}$$

In nonextensive statistics, the relation between the grand-canonical potential Ω_q and the grand-canonical partition function Z_q is similar to that in extensive statistics,

$$\Omega_q = -T\ln_q Z_q, \tag{15}$$

where the q-logarithm $\ln_q x$ is defined as [65]

$$\ln_q x \equiv \frac{x^{1-q}-1}{1-q}. \tag{16}$$

The derivation of Eq. (15) is presented in Appendix B.

It has been shown that in nonextensive statistics, thermodynamic consistency is also satisfied [20,29]. Thus, the pressure is given by

$$\begin{aligned} P_q &= -\frac{\Omega_q}{V} \\ &= \frac{T \ln_q Z_q}{V} \\ &= \frac{T}{V}\sum_{k=1}^{\infty} \ln_q \left[1 \pm \exp_q\left(-\frac{\varepsilon_k - \mu}{T}\right)\right]^{\pm d}, \end{aligned} \tag{17}$$

where the identity $\ln_q(x \otimes_q y) = \ln_q x + \ln_q y$ is used. In the large-volume limit, the summation in Eq. (17) is replaced by the integral in the six-dimensional phase space:

$$\sum_k \to V \int \frac{d^3k}{(2\pi)^3}. \tag{18}$$

Therefore, the pressure is rewritten as

$$P_q = T \int \frac{d^3k}{(2\pi)^3} \ln_q \left[1 \pm \exp_q\left(-\frac{\varepsilon_k - \mu}{T}\right)\right]^{\pm d}, \tag{19}$$

where $\varepsilon_k = \sqrt{m^2 + k^2}$, and m and k are, respectively, the rest mass and the momentum of the particle.

The entropy density for a multicomponent system with N number of species, then, is expressed as

$$s_q = \sum_{i=1}^{N} \partial P_q^i / \partial T, \tag{20}$$

where P_q^i is the pressure for the single-component system with the particle type i. One key factor in the calculation of the entropy density is the number of internal degrees of freedom d. In the QGP (hadronic) phase, the masses of u, d, and s quarks (hadrons and resonances composed of these quarks) are considered. The degeneracy factor for quarks (antiquarks) of a given flavor is $d_{q(\bar{q})} = 2_{\mathrm{spin}} \times N_c = 6$, while for gluons the degeneracy is $d_g = 2_{\mathrm{spin}} \times (N_c^2 - 1) = 16$, where $N_c = 3$ represents the number of colors. For hadrons of a specific species, the degeneracy factor is given by $d_H = 2S + 1$, with S denoting the spin of the hadron. Another key factor in the calculation of the entropy density is the chemical potential. The chemical potential for the ith particle species is $\mu_i = B_i\mu_B + S_i\mu_S + Q_i\mu_Q$, where B_i, S_i, and Q_i are, respectively, the particle's baryon, strangeness, and electric charge numbers, while μ_B, μ_S, and μ_Q are the respective chemical potentials of the system.

C. Smooth crossover around the critical temperature

In Sec. II B, the EOS in the hadronic (QGP) phase has been constructed by applying a nonextensive correction to the hadron resonance (parton) gas model. In order to match the equations of state in the hadronic and QGP phases around the crossover temperature T_c, we make a smooth interpolation of $s_q(T)$ between the hadronic gas at low T and the QGP at high T. The simplest possible parametrization of the entropy density $s_q(T)$ satisfying the thermodynamic inequality $\partial s_q(T)/\partial T \geq 0$ and the third law of thermodynamics, $s_q(T \to 0) \to$ constant, is [12]

$$s_q(T) = f(T) s_q^{\mathrm{H}}(T) + (1 - f(T)) s_q^{\mathrm{QGP}}(T), \tag{21}$$

where $f(T)$ is a weighting function,

$$f(T) = \frac{1}{2}[1 - \tanh((T - T_c)/\Gamma)], \tag{22}$$

with Γ setting the width of the phase transition region. For T satisfying $|T - T_c| > \Gamma$, $s_q(T)$ quickly approaches s_q^{H} below T_c and s_q^{QGP} above T_c.

The pressure $P_q(T)$, the energy density $\varepsilon_q(T)$, the specific heat at constant volume $(C_V)_q(T)$, and the squared speed of sound $(c_s^2)_q(T)$ then can be obtained using the following expressions, respectively:

$$P_q(T) = \int_0^T s_q(t) dt, \tag{23}$$

$$\varepsilon_q(T) = T s_q(T) - P_q(T) + \sum_i \mu_i \int_0^T \frac{\partial s_q(t)}{\partial \mu_i} dt, \tag{24}$$

$$(C_V)_q(T) = \left.\frac{\partial \varepsilon_q(T)}{\partial T}\right|_V = T\frac{\partial s_q(T)}{\partial T} + \sum_i \mu_i \frac{\partial s_q(T)}{\partial \mu_i}, \tag{25}$$

$$(c_s^2)_q(T) = \frac{\partial P_q(T)}{\partial \varepsilon_q(T)} = \frac{s_q(T)}{(C_V)_q(T)}, \tag{26}$$

where the index i in the summation runs over all the particle species.

III. RESULTS AND DISCUSSIONS

A. Zero chemical potential

The QCD phase transition is first studied at zero chemical potential. In the QGP phase, the u, d, and s quarks are considered, with masses set to $m_u = 3.503\ \mathrm{MeV}/c^2$, $m_d = 3.503\ \mathrm{MeV}/c^2$, and $m_s = 96.4\ \mathrm{MeV}/c^2$, respectively [66]. In the hadronic phase, hadrons and hadron resonances composed of u, d, and s quarks with masses below $2.5\ \mathrm{GeV}/c^2$ [16] from the Particle Data Group [67] are considered.

In each subplot of Fig. 1, the dashed and solid black curves present dimensionless thermodynamic quantities such as the entropy density s_q/T^3, the pressure P_q/T^4, the energy density ε_q/T^4, the specific heat at constant volume $(C_V)_q/T^3$, the trace anomaly $\Delta_q = (\varepsilon_q - 3P_q)/T^4$, and the squared speed of sound $(c_s^2)_q$ as a function of the temperature for two nonextensive parameters, $q = 1$ and $q = 1.05$, respectively. In the figure, T_c is taken to be

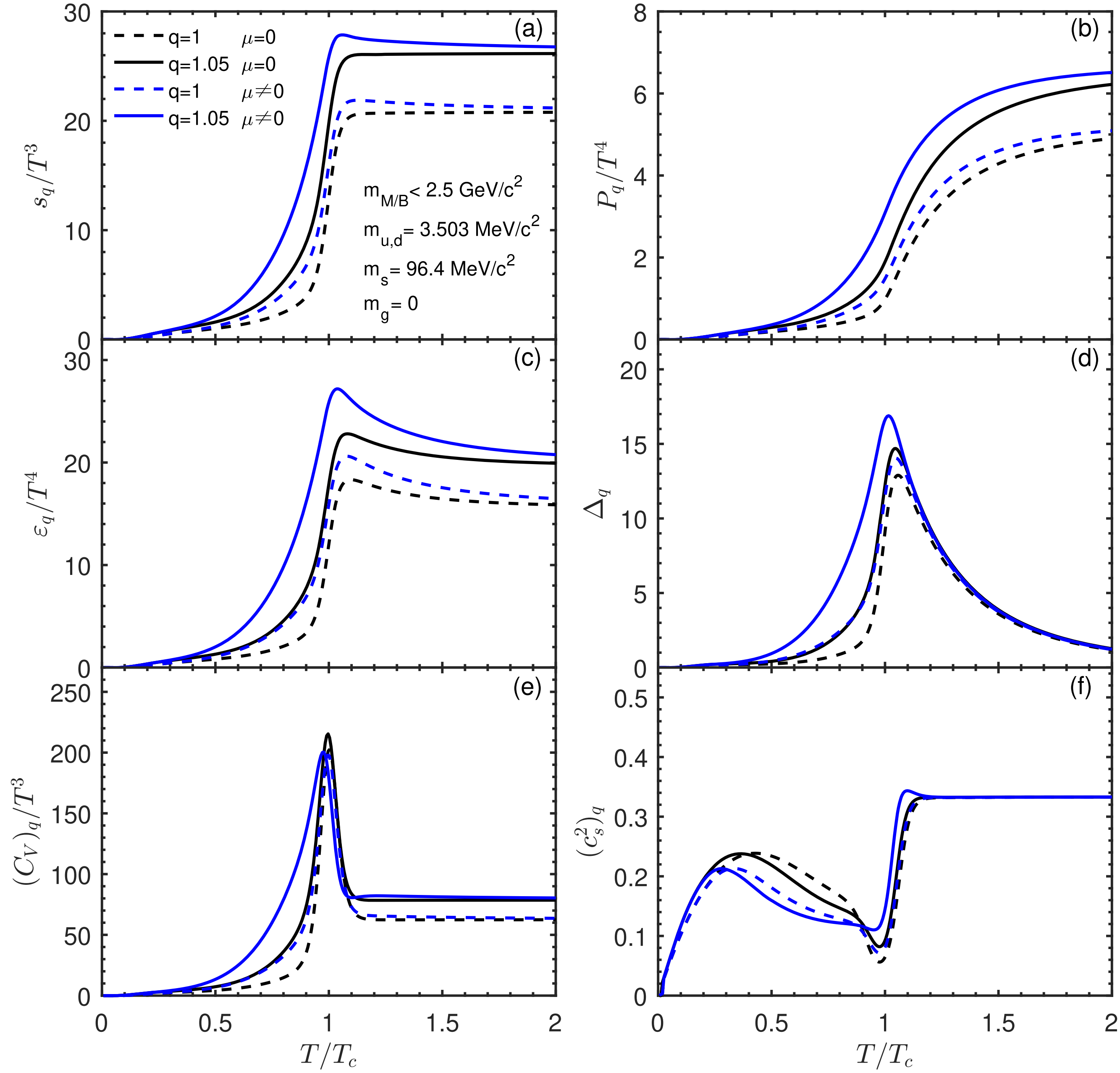

FIG. 1. (a) s_q/T^3, (b) P_q/T^4, (c) ε_q/T^4, (d) Δ_q, (e) $(C_V)_q/T^3$, and (f) $(c_s^2)_q$ as functions of T/T_c. The solid and dashed black lines correspond to $q = 1.05$ and $q = 1$, respectively, with zero chemical potential. The solid and dashed blue lines correspond to $q = 1.05$ and $q = 1$, respectively, with $\mu_B = 398.2$ MeV, $\mu_S = 89.5$ MeV, and $\mu_Q = 0$ MeV.

156.5 MeV [68], and Γ is set as $0.05T_c$, which is identical to the choice made in Ref. [12]. The qualitative behavior of these thermodynamic quantities in both cases can be summarized as follows:

(i) There is a rapid increase of the entropy density in a narrow region of T around T_c (with a width ∼8 MeV). In the high-temperature region, s_q/T^3 approaches the Stefan-Boltzmann (SB) limit. In the low-temperature region, s_q/T^3 approaches 0. This behavior could be explained as follows: The excitation of a massive hadron of mass m is exponentially suppressed by the Boltzmann factor $\exp(-m/T)$. The entropy density s_q is dominated by this exponential factor, which vanishes much more rapidly than the power-law term T^3 when $T \to 0$.

(ii) P_q/T^4 increases rather slowly with $T > T_c$ and approaches the SB limit at high temperature. As shown in Eq. (23), $P_q(T)$ is expressed as an integral of $s_q(T)$, thus such a continuous and slow rise is naturally expected [12].

(iii) There is a peak just above T_c for the temperature dependence of ε_q/T^4. The existence of such a peak is due to the rapid increase of $s_q(T)$ and the slow rise of $P_q(T)$ above T_c [12].

(iv) $(C_V)_q/T^3$ has an obvious peak near T_c. The specific heat at constant volume is defined as the derivative of the energy density with respect to the temperature. The dimensionless ε_q/T^4 has a peak above T_c, which leads to the peak of $(C_V)_q/T^3$ near T_c.

(v) Δ_q also has a prominent peak near T_c. Such a peak is a consequence of the rapid increase of $s_q(T)$. It vanishes when the temperature approaches either 0 or ∞.

(vi) s_q/T^3, P_q/T^4, ε_q/T^4, $(C_V)_q/T^3$, and Δ_q are sensitive to the deviation of q from unity, and they become large both in the hadronic and QGP phases with the increase of q. This can be interpreted as the effect that at a fixed temperature, the particle yield in the nonextensive distribution with $q > 1$ is always larger than that in the extensive one.

(vii) $(c_s^2)_q$ exhibits a sharp drop in the critical region $|T - T_c| < \Gamma$ and stays below $1/3$ in the hadronic phase. In both cases, the behavior results from the energy density $\varepsilon_q(T)$ rising more rapidly than the pressure $P_q(T)$, leading to a soft equation of state. Across T_c, this is due to deconfinement. In the hadronic phase, it is a consequence of hadron masses. Moreover, $(c_s^2)_q$ approaches $1/3$ in the high-temperature region and 0 in the low-temperature region. This could be understood as follows: At low temperatures, the exponential suppression $\exp(-m/T)$ causes both P_q and ε_q to vanish, but their derivatives vanish at different rates. The ratio of these derivatives, $(c_s^2)_q = \partial P_q/\partial \varepsilon_q$, scales as T/m, guaranteeing it approaches zero with $T \to 0$. At extremely high temperatures, the masses of the u, d, and s are negligible. Thus, these quarks behave dynamically as massless noninteracting particles. Additionally, the deviation of q from unity leads to nontrivial corrections of the squared speed of sound in the vicinity of the critical point and at lower temperatures.

We have also investigated the Γ dependence of the thermodynamic quantities at the vanishing chemical potential for both extensive and nonextensive cases in Fig. 2. The dashed (solid) black and blue curves represent the temperature dependence of these quantities with $\Gamma = 0.05T_c$ and $\Gamma = 0.25T_c$, respectively, for the extensive (nonextensive) cases. It is observed that an increase in the value of Γ leads to a more gradual temperature dependence of the entropy density and pressure. Concurrently, the characteristic peaks in the trace anomaly and the specific heat at constant volume undergo a broadening and a reduction in height. For the squared speed of sound, an increase in Γ produces a dip that is both shallower and significantly wider. This set of phenomena is attributable to the broadening of the QCD phase transition window. Specifically, a larger Γ implies that the conversion from the hadronic phase to the QGP phase takes place across an extended temperature interval, which smears out the thermodynamic profiles, resulting in smoother, broader, and flatter curves.

B. Finite chemical potential

The QCD phase transition is also investigated at finite chemical potential. The baryon, strangeness, and electric charge potentials are, respectively, set as $\mu_B = 398.2$ MeV, $\mu_S = 89.5$ MeV, and $\mu_Q = 0$ MeV, which correspond to the chemical potentials of the system created in the central Au-Au collisions at $\sqrt{s_{\rm NN}} = 7.7$ GeV [69]. In each subplot of Fig. 1, the solid and dashed blue curves show the temperature dependence of the thermodynamic quantities with finite chemical potential for $q = 1.05$ and $q = 1$, respectively. For the case with finite chemical potential, T_c and Γ are set to be the same values as those for the case with vanishing chemical potential. The qualitative behaviors of the thermodynamic quantities are summarized as follows:

(i) s_q/T^3, P_q/T^4, ε_q/T^4, $(C_V)_q/T^3$, and Δ_q are sensitive to the deviation of the chemical potential from zero, and they become large in both the hadronic and QGP phases with the increase of μ. This is due to the fact that at a given temperature, a larger population is expected for the system with finite chemical potential. A similar increase was observed for the normalized pressure and trace anomaly obtained from the Dyson-Schwinger equations when the values of quark chemical potential were increased [70].

(ii) With the increase of the chemical potential, the squared speed of sound $(c_s^2)_q$ increases in the vicinity of T_c and decreases at lower temperatures, which is different from the chemical potential dependence of s_q/T^3, P_q/T^4, ε_q/T^4, $(C_V)_q/T^3$, and Δ_q.

(iii) At high temperature, these thermodynamic quantities with finite chemical potential approach the respective ones with zero chemical potential. At low temperature, the thermodynamic quantities with both zero and finite chemical potential approach 0 when $T \to 0$.

(iv) As shown in the previous section, at zero chemical potential, the thermodynamic quantities are sensitive to the deviation of q from unity. With the consideration of effects of both the finite chemical potential and the nonextensivity, an obvious change of the behavior for the thermodynamic quantities is observed.

C. Comparison with other models

The upper panel of Fig. 3 displays the comparison of the temperature dependence of P_q/T^4 calculated with zero

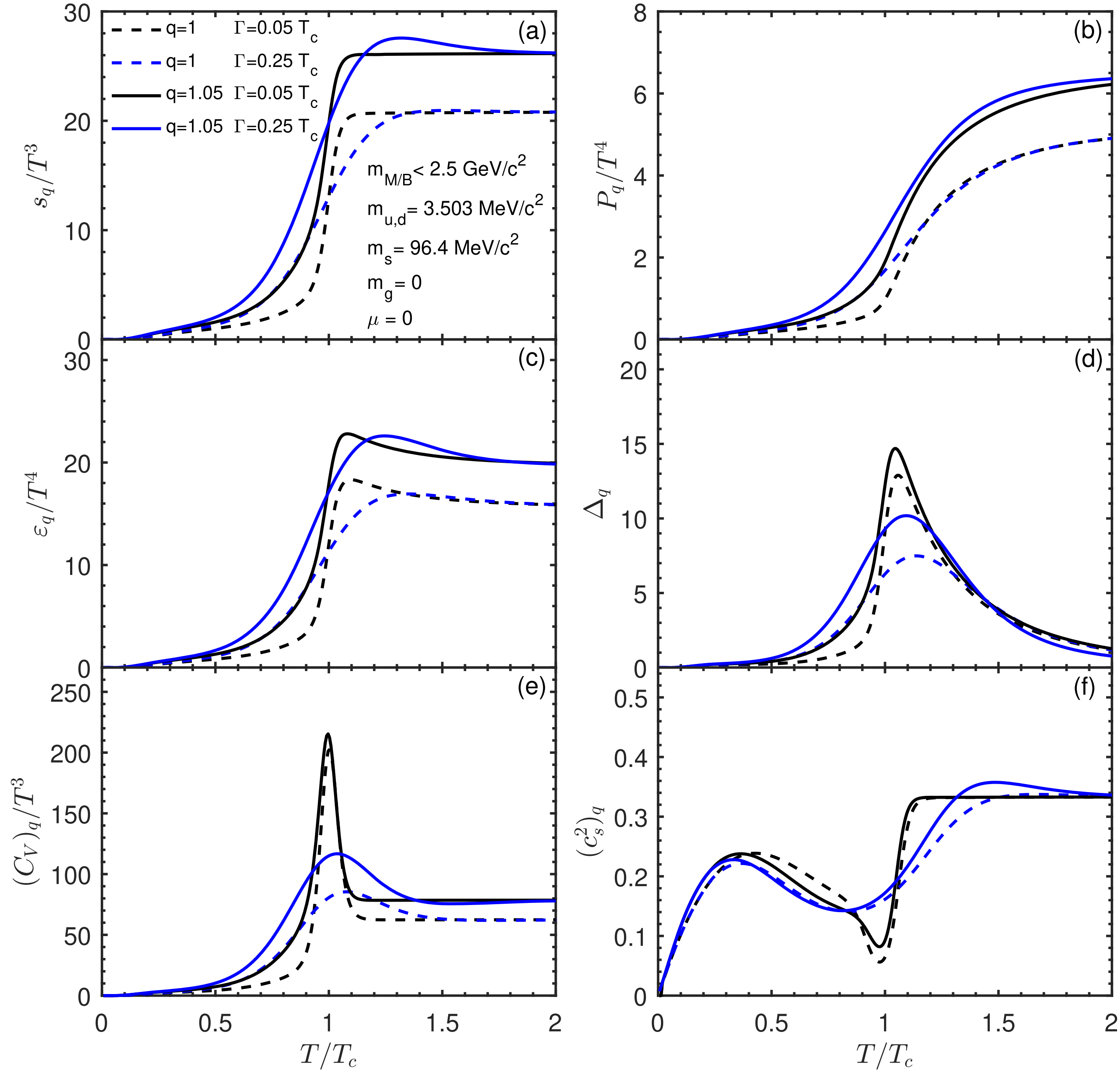

FIG. 2. (a) s_q/T^3, (b) P_q/T^4, (c) ε_q/T^4, (d) Δ_q, (e) $(C_V)_q/T^3$, and (f) $(c_s^2)_q$ as functions of T/T_c at zero chemical potential. The dashed (solid) black and blue curves represent the temperature dependence of these quantities with $\Gamma = 0.05T_c$ and $\Gamma = 0.25T_c$, respectively, for the extensive (nonextensive) cases.

chemical potential for different models. Our results with $q = 1.05$ and $q = 1$ are presented as solid and dashed lines, respectively. The result from the HRG model is shown as a dotted line, while the result from the LQCD is presented as solid black circles. The dependence extracted from the fit of experimental yields of hadrons at the central centrality in pp collisions at $\sqrt{s} = 7$ TeV [71–73] and 13 TeV [74,75], p-Pb collisions at $\sqrt{s_{\mathrm{NN}}} = 5.02$ TeV [76–78], Pb-Pb collisions at $\sqrt{s_{\mathrm{NN}}} = 2.76$ TeV [79–82] and 5.02 TeV [83,84], and Xe-Xe collisions at $\sqrt{s_{\mathrm{NN}}} = 5.44$ TeV [85] using the Thermal-Fist package [61] are shown as empty markers. Thermal-Fist is a C++ package designed for the analyses of particle productions in relativistic heavy-ion collisions within the framework of the HRG model. In the package, there are several options regarding the ensemble with which to treat the baryon number, strangeness, and electric charge. In this work, we choose the grand-canonical ensemble, which is widely applied to heavy-ion collisions [86–89]. It is shown that our result with $q = 1$ agrees well with the HRG model and the LQCD data up to $T \sim 150$ MeV. In our model, $P_q(T)$ quickly approaches the pressure at the hadronic phase with $T < T_c - \Gamma$. When $q \to 1$, the Tsallis

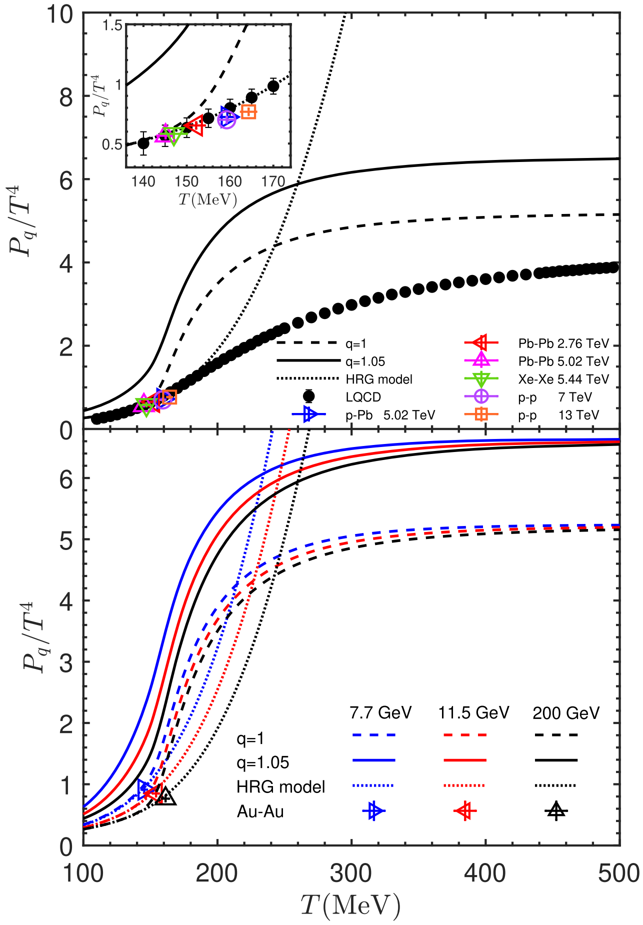

FIG. 3. Upper panel: P_q/T^4 as a function of T with zero chemical potential for $q = 1.05$ (the solid line) and 1 (the dashed line). The results from the HRG model, the LQCD, and the Thermal-Fist fit are shown as the dotted line, the solid black circles, and the empty markers, respectively. The inset is the temperature dependence of P_q/T^4 in the region with 136 MeV $< T <$ 174 MeV. Lower panel: P_q/T^4 as a function of T with finite chemical potential for $q = 1.05$ (the solid line) and $q = 1$ (the dashed line). The results from the HRG model and the Thermal-Fist fit are, respectively, shown as the dotted line and the empty markers.

statistics approaches the BG statistics valid for systems under the thermal equilibrium. Thus, the agreement at low temperature is reasonably expected, as the HRG model and the LQCD calculations are based on equilibrium considerations. Moreover, our result with $q = 1$ is consistent with the results from the Thermal-Fist fit to the hadron yields at the central centrality in Pb-Pb collisions at $\sqrt{s_{\mathrm{NN}}} = 2.76$ TeV (triangle-left) and 5.02 TeV (triangle-up), and in Xe-Xe collisions at $\sqrt{s_{\mathrm{NN}}} = 5.44$ TeV (triangle-down). However, it obviously overestimates the results from the Thermal-Fist fit to the hadron yields in p-Pb collisions at $\sqrt{s_{\mathrm{NN}}} = 5.02$ TeV (triangle-right), and in pp collisions at $\sqrt{s} = 7$ TeV (empty circle) and 13 TeV (empty square). In pp and p-Pb collisions, the temperature of the system is around 160 MeV, which is

TABLE I. Chemical potentials in central Au-Au collisions at $\sqrt{s_{\mathrm{NN}}} = 7.7$, 11.5, and 200 GeV.

$\sqrt{s_{\mathrm{NN}}}$ (GeV)	Centrality	μ_B (MeV)	μ_S (MeV)	μ_Q (MeV)
7.7	0%–5%	398.2	89.5	0
11.5	0%–5%	287.3	64.5	0
200	0%–5%	28.4	5.6	0

in the phase transition region $|T - T_c| < \Gamma$, leading to the overestimate of our model for the pressure. At high temperature, our result approaches the SB limit of the pressure for idea parton gas. However, in LQCD, partons interact with each other, which leads to the deviation from the limit. In the HRG model, only the hadron gas is considered and the phase transition is absent; thus, the pressure approaches infinity at high temperature.

The lower panel of Fig. 3 shows the comparison of the temperature dependence of P_q/T^4 calculated with three sets of finite chemical potentials (see Table I) for different models. They correspond to the chemical potentials in central Au-Au collisions at $\sqrt{s_{\mathrm{NN}}} = 7.7$, 11.5, and 200 GeV [69]. Our results with $q = 1.05$ and $q = 1$ are, respectively, presented as the solid and dashed lines. The results from the HRG model are shown as the dotted line. The results extracted from the Thermal-Fist fit of experimental yields of hadrons in central Au-Au collisions at $\sqrt{s_{\mathrm{NN}}} = 7.7$, 11.5, and 200 GeV [69,90–92] are shown as empty blue, red, and black markers, respectively. It is found that our results with $q = 1$ agree well with the HRG model up to $T \sim 150$ MeV. Moreover, our results with $q = 1$ are consistent with the results from the Thermal-Fist fit to the hadron yields in central Au-Au collisions at $\sqrt{s_{\mathrm{NN}}} = 7.7$ GeV (triangle-right) and 11.5 GeV (triangle-left). However, they overestimate the result from the Thermal-Fist fit to the hadron yields in central Au-Au collisions at $\sqrt{s_{\mathrm{NN}}} = 200$ GeV (triangle-up). The temperature of the system in Au-Au collisions at $\sqrt{s_{\mathrm{NN}}} =$ 200 GeV is around 160 MeV, falling in the phase transition region and leading to this overestimate.

IV. CONCLUSIONS

In this work, by applying the nonextensive correction to the EOS in the parton (hadron resonance) gas at high (low) temperature and making a smooth interpolation of these two equations of state, we have constructed a nonextensive version of the EOS to investigate the properties of QCD phase transition with both zero and nonzero chemical potentials. We find that the dimensionless quantities such as s_q/T^3, P_q/T^4, ε_q/T^4, $(C_V)_q/T^3$, and Δ_q are highly sensitive to the nonextensivity parameter q. As q deviates from unity, these quantities increase in both the hadronic and QGP phases. Furthermore, this deviation introduces nontrivial corrections to $(c_s^2)_q$ near the critical point and at lower temperatures. These thermodynamic quantities also exhibit significant sensitivity to the chemical potential μ. They increase with μ in both phases. Specifically, $(c_s^2)_q$ rises near the phase transition temperature but decreases at lower temperatures. Finally, we observe that our results with $q = 1$ agree well with the LQCD, the HRG, and the results from the Thermal-Fist fit to the hadron yield in high-energy nuclear collisions in the low-temperature region up to $T \sim 150$ MeV. These findings will deepen our understanding for the properties of the QCD phase transition at finite temperature and chemical potential, both in the extensive and nonextensive statistics.

ACKNOWLEDGMENTS

This work is supported by the Scientific Research Foundation for the Returned Overseas Chinese Scholars, State Education Ministry, by the Natural Science Basic Research Plan in Shaanxi Province of China (Program No. 2023-JC-YB-012), and by the National Natural Science Foundation of China under Grants No. 11447024, No. 11505108, and No. 12275204.

DATA AVAILABILITY

The data that support the findings of this article are not publicly available upon publication, because it is not technically feasible and/or the cost of preparing, depositing, and hosting the data would be prohibitive within the terms of this research project. The data are available from the authors upon reasonable request.

APPENDIX A: THE DERIVATION OF EQS. (12) AND (13)

In the framework of the nonextensive statistics, the grand-canonical partition function of particles with d internal degrees of freedom is given by

$$Z_q = \left(\prod_{k=1}^{\infty}\right)_q \left[\sum_{n_k=0}^{\infty} \exp_q\left(-\frac{(\varepsilon_k - \mu)n_k}{T}\right)\right]^d, \quad \text{(A1)}$$

where ε_k and n_k are, respectively, the energy of a particle and the number of particles in the state k; T and μ are, respectively, the temperature and the chemical potential of the system.

For noninteracting fermions, their grand-canonical partition function is written as

$$\begin{aligned} Z_q^F &= \left(\prod_{k=1}^{\infty}\right)_q \left[\sum_{n_k=0}^{1} \exp_q\left(-\frac{(\varepsilon_k - \mu)n_k}{T}\right)\right]^d \\ &= \left(\prod_{k=1}^{\infty}\right)_q \left[1 + \exp_q\left(-\frac{(\varepsilon_k - \mu)}{T}\right)\right]^d. \end{aligned} \quad \text{(A2)}$$

For noninteracting bosons, their grand-canonical partition function is written as

$$\begin{aligned} Z_q^B &= \left(\prod_{k=1}^{\infty}\right)_q \left[\sum_{n_k=0}^{\infty} \exp_q\left(-\frac{(\varepsilon_k - \mu)n_k}{T}\right)\right]^d \\ &= \left(\prod_{k=1}^{\infty}\right)_q \left[1 + \cdots + \exp_q\left(-n_k\frac{\varepsilon_k - \mu}{T}\right) + \cdots\right]^d \\ &\approx \left(\prod_{k=1}^{\infty}\right)_q \left[1 - \exp_q\left(-\frac{\varepsilon_k - \mu}{T}\right)\right]^{-d}, \end{aligned} \quad \text{(A3)}$$

where the approximation $\exp_q(x)\exp_q(y) = \exp_q(x + y + (1-q)xy) \approx \exp_q(x+y)$ has been adopted [93].

APPENDIX B: THE DERIVATION OF EQ. (15)

In the grand-canonical ensemble, the probability distribution of the state R and the partition function in Eqs. (7) and (8) are, respectively, rewritten as

$$\begin{aligned} p_R &= \frac{1}{Z_q}\exp_q(-\alpha N_R - \beta E_R), \\ Z_R &= \sum_{R=1}^{W} \exp_q(-\alpha N_R - \beta E_R), \end{aligned} \quad \text{(B1)}$$

where $\alpha \equiv -\mu/T$, $\beta \equiv 1/T$, W is the total number of states.

The particle number N, the energy E, and the generalized force Y are then, respectively, given by

$$\begin{aligned} N &= \sum_R p_R^q N_R = \frac{\sum_R[\exp_q(-\alpha N_R - \beta E_R)]^q N_R}{Z_q^q} \\ &= -\frac{\partial}{\partial\alpha}\ln_q Z_q, \end{aligned} \quad \text{(B2)}$$

$$\begin{aligned} E &= \sum_i p_R^q E_R = \frac{\sum_R[\exp_q(-\alpha N_R - \beta E_R)]^q E_R}{Z_q^q} \\ &= -\frac{\partial}{\partial\beta}\ln_q Z_q, \end{aligned} \quad \text{(B3)}$$

$$\begin{aligned} Y &= \sum_R p_R^q \frac{\partial E_R}{\partial y} = \frac{\sum_R[\exp_q(-\alpha N_R - \beta E_R)]^q \frac{\partial E_R}{\partial y}}{Z_q^q} \\ &= -\frac{1}{\beta}\frac{\partial}{\partial y}\ln_q Z_q. \end{aligned} \quad \text{(B4)}$$

With Eqs. (B2)–(B4), the following relation is constructed:

$$\begin{aligned} &\beta\left(dE - Y dy + \frac{\alpha}{\beta}dN\right) \\ &= -\beta d\left(\frac{\partial \ln_q Z_q}{\partial\beta}\right) + \frac{\partial \ln_q Z_q}{\partial y}dy - \alpha d\left(\frac{\partial \ln_q Z_q}{\partial\alpha}\right). \end{aligned} \quad \text{(B5)}$$

Since $\ln_q Z_q$ is a function of α, β, and y, its full differential is

$$d(\ln_q Z_q) = \frac{\partial \ln_q Z_q}{\partial \beta} d\beta + \frac{\partial \ln_q Z_q}{\partial \alpha} d\alpha + \frac{\partial \ln_q Z_q}{\partial y} dy. \quad \text{(B6)}$$

Combing Eqs. (B5) and (B6), we can get

$$\begin{aligned} &\beta\left(dE - Ydy + \frac{\alpha}{\beta} dN\right) \\ &= d\left(\ln_q Z_q - \alpha \frac{\partial \ln_q Z_q}{\partial \alpha} - \beta \frac{\partial \ln_q Z_q}{\partial \beta}\right). \end{aligned} \quad \text{(B7)}$$

It has been shown that the following thermodynamic relation still holds in the nonextensive statistics [20,29]:

$$dS = \frac{1}{T}(dE - Ydy - \mu dN). \quad \text{(B8)}$$

Comparing Eq. (B7) with Eq. (B8), we obtain the entropy S as

$$S = \ln_q Z_q - \alpha \frac{\partial \ln_q Z_q}{\partial \alpha} - \beta \frac{\partial \ln_q Z_q}{\partial \beta}. \quad \text{(B9)}$$

Therefore, in the nonextensive statistics, the relation between the grand-canonical potential Ω and the grand-canonical partition function Z_q is

$$\begin{aligned} \Omega &= E - TS - \mu N \\ &= -\frac{\partial}{\partial \beta} \ln_q Z_q - \mu\left(-\frac{\partial}{\partial \alpha} \ln_q Z_q\right) \\ &\quad - T\left(\ln_q Z_q - \alpha \frac{\partial \ln_q Z_q}{\partial \alpha} - \beta \frac{\partial \ln_q Z_q}{\partial \beta}\right) \\ &= -T \ln_q Z_q. \end{aligned} \quad \text{(B10)}$$

[1] A. Chodos, R. L. Jaffe, K. Johnson, C. B. Thorn, and V. F. Weisskopf, New extended model of hadrons, Phys. Rev. D **9**, 3471 (1974).

[2] Y. Nambu and G. Jona-Lasinio, Dynamical model of elementary particles based on an analogy with superconductivity. I, Phys. Rev. **122**, 345 (1961).

[3] Y. Nambu and G. Jona-Lasinio, Dynamical model of elementary particles based on an analogy with superconductivity. II, Phys. Rev. **124**, 246 (1961).

[4] M. N. Chernodub and A. S. Nedelin, Phase diagram of chirally imbalanced QCD matter, Phys. Rev. D **83**, 105008 (2011).

[5] B. J. Schaefer, J. M. Pawlowski, and J. Wambach, Phase structure of the Polyakov-quark-meson model, Phys. Rev. D **76**, 074023 (2007).

[6] B. J. Schaefer, M. Wagner, and J. Wambach, Thermodynamics of (2+1)-flavor QCD: Confronting models with lattice studies, Phys. Rev. D **81**, 074013 (2010).

[7] C. D. Roberts and A. G. Williams, Dyson-Schwinger equations and their application to hadronic physics, Prog. Part. Nucl. Phys. **33**, 477 (1994).

[8] C. D. Roberts and S. M. Schmidt, Dyson-Schwinger equations: Density, temperature and continuum strong QCD, Prog. Part. Nucl. Phys. **45**, S1 (2000).

[9] C. Wetterich, Exact evolution equation for the effective potential, Phys. Lett. B **301**, 90 (1993).

[10] N. Dupuis, L. Canet, A. Eichhorn, W. Metzner, J. M. Pawlowski, M. Tissier, and N. Wschebor, The nonperturbative functional renormalization group and its applications, Phys. Rep. **910**, 1 (2021).

[11] J.-X. Shao, W.-J. Fu, and Y.-X. Liu, Chemical freeze-out parameters via a functional renormalization group approach, Phys. Rev. D **109**, 034019 (2024).

[12] M. Asakawa and T. Hatsuda, What thermodynamics tells us about the QCD plasma, Phys. Rev. D **55**, 4488 (1997).

[13] F. Karsch, K. Redlich, and A. Tawfik, Hadron resonance mass spectrum and lattice QCD thermodynamics, Eur. Phys. J. C **29**, 549 (2003).

[14] P. Huovinen and P. Petreczky, QCD equation of state and hadron resonance gas, Nucl. Phys. **A837**, 26 (2010).

[15] A. Bazavov *et al.* (HotQCD Collaboration), Fluctuations and correlations of net baryon number, electric charge, and strangeness: A comparison of lattice QCD results with the hadron resonance gas model, Phys. Rev. D **86**, 034509 (2012).

[16] A. Bazavov *et al.* (HotQCD Collaboration), Equation of state in (2+1)-flavor QCD, Phys. Rev. D **90**, 094503 (2014).

[17] S. Borsanyi, Z. Fodor, C. Hoelbling, S. D. Katz, S. Krieg, and K. K. Szabó, Full result for the QCD equation of state with 2+1 flavors, Phys. Lett. B **730**, 99 (2014).

[18] G. Wilk and Z. Wlodarczyk, Interpretation of the nonextensivity parameter q in some applications of Tsallis statistics and lévy distributions, Phys. Rev. Lett. **84**, 2770 (2000).

[19] T. S. Biro and A. Jakovac, Power-law tails from multiplicative noise, Phys. Rev. Lett. **94**, 132302 (2005).

[20] T. Osada and G. Wilk, Nonextensive hydrodynamics for relativistic heavy-ion collisions, Phys. Rev. C **77**, 044903 (2008).

[21] M. Ruggeieri, Pooja, J. Prakash, and S. K. Das, Memory effects on energy loss and diffusion of heavy quarks in the quark-gluon plasma, , Phys. Rev. D **106**, 034032 (2022).

[22] A. Dragoa, A. Lavagno, and P. Quarati, Nonextensive statistical effects on the relativistic nuclear equation of state, Physica (Amsterdam) **344A**, 472 (2004).

[23] T. S. Biro and G. Purcsel, Nonextensive statistical effects on the relativistic nuclear equation of state, Phys. Rev. Lett. **95**, 162302 (2005).

[24] T. S. Biro and G. Purcsel, Equilibration of two power-law tailed distributions in a parton cascade model, Phys. Lett. A **372**, 1174 (2008).

[25] C. Tsallis, Possible generalization of Boltzmann-Gibbs statistics, J. Stat. Phys. **52**, 479 (1988).

[26] A. Deppman, Thermodynamics with fractal structure, Tsallis statistics, and hadrons, Phys. Rev. D **93**, 054001 (2016).

[27] A. Deppman, E. Megias, and D. P. Menezes, Fractals, nonextensive statistics, and QCD, Phys. Rev. D **101**, 034109 (2020).

[28] J. Cleymans and D. Worku, Relativistic thermodynamics: Transverse momentum distributions in high-energy physics, Eur. Phys. J. A **48**, 160 (2012).

[29] J. Cleymans and D. Worku, The Tsallis distribution in proton-proton collisions at $\sqrt{s} = 0.9$ TeV at the LHC, J. Phys. G **39**, 025006 (2012).

[30] J. Adams *et al.* (STAR Collaboration), Identified hadron spectra at large transverse momentum in pp and d+Au collisions at $\sqrt{s_{\mathrm{NN}}} = 200$ GeV, Phys. Lett. B **637**, 161 (2006).

[31] A. Adare *et al.* (PHENIX Collaboration), Nuclear modification factors of ϕ mesons in d+Au, Cu+Cu, and Au+Au collisions at $\sqrt{s_{\mathrm{NN}}} = 200$ GeV, Phys. Rev. C **83**, 024909 (2011).

[32] W.-C. Zhang and C.-B. Yang, Scaling behaviour of charged hadron distributions in pp and $p\bar{p}$-collisions, J. Phys. G **41**, 105006 (2014).

[33] S. Chatrchyan *et al.* (ALICE Collaboration), Study of the production of charged pions, kaons, and protons in pPb collisions at $\sqrt{s_{\mathrm{NN}}} = 5.02$ TeV, Eur. Phys. J. C **74**, 2847 (2014).

[34] M. D. Azmi and J. Cleymans, Transverse momentum distributions at the LHC and Tsallis thermodynamics, Acta Phys. Pol. B Proc. Suppl. **7**, 9 (2014).

[35] H. Zheng and L. Zhu, Transverse momentum distributions at the lhc and tsallis thermodynamicscan tsallis distribution fit all the particle spectra produced at RHIC and LHC?, Adv. High Energy Phys. **2015**, 180491 (2015).

[36] W.-C. Zhang, Scaling behaviours of the p_{T} spectra for identified hadrons in pp collisions, J. Phys. G **43**, 015003 (2016).

[37] J. Cleymans, G. I. Lykasov, A. S. Parvan, A. S. Sorin, O. V. Teryaev, and D. Worku, Systematic properties of the Tsallis distribution: Energy dependence of parameters in high energy $p-p$ collisions, Phys. Lett. B **723**, 351 (2013).

[38] M. D. Azmi and J. Cleymans, Transverse momentum distributions in proton–proton collisions at LHC energies and Tsallis thermodynamics, J. Phys. G **41**, 065001 (2014).

[39] M. D. Azmi and J. Cleymans, The Tsallis distribution at large transverse momenta, Eur. Phys. J. C **75**, 430 (2015).

[40] L. Marques, J. Cleymans, and A. Deppman, Description of high-energy pp collisions using Tsallis thermodynamics: Transverse momentum and rapidity distributions,, Phys. Rev. D **91**, 054025 (2015).

[41] H. Zheng, L. Zhu, and A. Bonasera, Systematic analysis of hadron spectra in $p+p$ collisions using Tsallis distributions, Phys. Rev. D **92**, 074009 (2015).

[42] A. Khuntia, S. Tripathy, R. Sahoo, and J. Cleymans, Multiplicity dependence of non-extensive parameters for strange and multi-strange particles in proton-proton collisions at $\sqrt{s} = 7$ TeV at the LHC, Eur. Phys. J. A **53**, 103 (2017).

[43] L.-Y. Qiao, G.-R. Che, J.-B. Gu, H. Zheng, and W.-C. Zhang, Nuclear modification factor in Pb–Pb and p-Pb collisions using Boltzmann transport equation, J. Phys. G **47**, 075101 (2020).

[44] G.-R. Che, J.-B. Gu, W.-C. Zhang, and H. Zheng, Identified particle spectra in Pb–Pb, Xe–Xe and p–Pb collisions with the Tsallis blast-wave model, J. Phys. G **48**, 095103 (2021).

[45] J.-B. Gu, C.-Y. Li, Q. Wang, W.-C. Zhang, and H. Zheng, Collective expansion in pp collisions using the Tsallis statistics, J. Phys. G **49**, 115101 (2022).

[46] F. S. Navarra, O. V. Utyuzh, G. Wilk, and Z. Wlodarczyk, Estimating inelasticity with the information theory approach, Phys. Rev. D **67**, 114002 (2003).

[47] M. Alqahtani, N. Demir, and M. Strickland, Nonextensive hydrodynamics of boost-invariant plasmas, Eur. Phys. J. C **82**, 973 (2022).

[48] K. Kyan and A. Monnai, QCD equation of state with Tsallis statistics for heavy-ion collisions, Phys. Rev. D **106**, 054004 (2022).

[49] J.-H. Shi, Z.-Y. Qin, J.-P. Zhang, J. Cao, Z.-F. Jiang, W.-C. Zhang, and H. Zheng, Nonextensive (3+1)-dimensional hydrodynamics for relativistic heavy-ion collisions, Phys. Rev. D **111**, 036010 (2025).

[50] P. Arnold, J. Lenaghan, G. D. Moore, and L. G. Yaffe, Apparent thermalization due to plasma instabilities in the quark-gluon plasma, Phys. Rev. Lett. **94**, 072302 (2005).

[51] A. Takacs and D. Molnar, Suppression of elliptic flow without viscosity, arXiv:1906.12311.

[52] A. M. Teweldeberhan, H. G. Miller, and R. Tegen, Generalized statistics and the formation of a quark-gluon plasma, Int. J. Mod. Phys. E **12**, 395 (2003).

[53] F. I. M. Pereira, R. Silva, and J. S. Alcaniz, Nonextensive effects on the relativistic nuclear equation of state, Phys. Rev. C **76**, 015201 (2007).

[54] A. Lavagno, D. Pigato, and P. Quarati, Nonextensive statistical effects in the hadron to quark–gluon phase transition, J. Phys. G **37**, 115102 (2010).

[55] J. Rozynek and G. Wilk, Nonextensive effects in the Nambu–Jona-Lasinio model of QCD, J. Phys. G **36**, 125108 (2009).

[56] J. Rozynek and G. Wilk, Nonextensive Nambu-Jona-Lasinio Model of QCD matter, Eur. Phys. J. A **52**, 13 (2016).

[57] Y.-P. Zhao, Thermodynamic properties and transport coefficients of QCD matter within the nonextensive Polyakov–Nambu–Jona-Lasinio model, Phys. Rev. D **101**, 096006 (2020).

[58] Y.-P. Zhao, S.-Y. Zuo, and C.-M. Li, QCD chiral phase transition and critical exponents within the nonextensive Polyakov-Nambu-Jona-Lasinio model, Chin. Phys. C **45**, 073105 (2021).

[59] R. Hagedorn, Statistical dynamics of strong interactions at high energies, Nuovo Cimento Suppl. **3**, 147 (1965), http://cds.cern.ch/record/346206.

[60] J. Kapusta and C. Gale, *Finite Temperature Field Theory: Principles and Applications*, Cambridge Monographs on Mathematical Physics (Cambridge University Press, Cambridge, England, 2006).

[61] V. Vovchenko and H. Stoecker, Thermal-FIST: A package for heavy-ion collisions and hadronic equation of state, Comput. Phys. Commun. **244**, 295 (2019).

[62] C. Tsallis, Possible generalization of Boltzmann-Gibbs statistics, J. Stat. Phys. **52**, 479 (1988).
[63] S. Mitra, Thermodynamics and relativistic kinetic theory for q-generalized Bose-Einstein and Fermi-Dirac systems, Eur. Phys. J. C **78**, 66 (2018).
[64] L. D. Landau and E. M. Lifshitz, *Statistical Physics*, 3rd ed. (Pergamon, Oxford, 1980).
[65] C. Tsallis, R. S. Mendes, and A. R. Plastino, The role of constraints within generalized nonextensive statistics, Physica (Amsterdam) **261A**, 534 (1998).
[66] S. Durr, Z. Fodor, C. Hoelbling, S. D. Katz, S. Krieg, T. Kurth, L. Lellouch, T. Lippert, K. K. Szabo, and G. Vulvert (BMW Collaboration), Lattice QCD at the physical point: Light quark masses, Phys. Lett. B **701**, 265 (2011).
[67] C. Patrignani *et al.* (Particle Data Group), Review of Particle Physics, Chin. Phys. C **40**, 100001 (2016).
[68] A. Bazavov *et al.* (HotQCD Collaboration), Chiral crossover in QCD at zero and non-zero chemical potentials, Phys. Lett. B **795**, 15 (2019).
[69] L. Adamczyk *et al.* (STAR Collaboration), Bulk properties of the medium produced in relativistic heavy-ion collisions from the beam energy scan program, Phys. Rev. C **96**, 044904 (2017).
[70] F. Gao, J. Chen, Y.-X. Liu, S.-X. Qin, C. D. Roberts, and S. M. Schmidt, Phase diagram and thermal properties of strong-interaction matter, Phys. Rev. D **93**, 094019 (2016).
[71] S. Acharya *et al.* (ALICE Collaboration), Multiplicity dependence of light-flavor hadron production in pp collisions at $\sqrt{s} = 7$ TeV, Phys. Rev. C **99**, 024906 (2019).
[72] J. Adam *et al.* (ALICE Collaboration), Enhanced production of multi-strange hadrons in high-multiplicity proton–proton collisions, Nat. Phys. **13**, 535 (2017).
[73] B. Abele *et al.* (ALICE Collaboration), Enhanced production of multi-strange hadrons in high-multiplicity protonproton collisions at $\sqrt{s} = 7$ TeV with ALICE, Phys. Lett. B **712**, 309 (2012).
[74] S. Acharya *et al.* (ALICE Collaboration), Multiplicity dependence of π, K, and p production in pp collisions at $\sqrt{s} = 13$ TeV, Eur. Phys. J. C **80**, 693 (2020).
[75] S. Acharya *et al.* (ALICE Collaboration), Multiplicity dependence of $K^*(892)^0$ and $\phi(1020)$ production in pp collisions at $\sqrt{s} = 13$ TeV, Phys. Lett. B **807**, 135501 (2020).
[76] B. Abele *et al.* (ALICE Collaboration), Multiplicity dependence of pion, kaon, proton and lambda production in pPb collisions at $\sqrt{s_{\mathrm{NN}}} = 5.02$ TeV, Phys. Lett. B **728**, 25 (2014).
[77] J. Adam *et al.* (ALICE Collaboration), Multi-strange baryon production in p-Pb collisions at $\sqrt{s_{\mathrm{NN}}} = 5.02$ TeV, Phys. Lett. B **758**, 389 (2016).
[78] J. Adam *et al.* (ALICE Collaboration), Production of $K^*(892)^0$ and $\phi(1020)$ production in pPb collisions at $\sqrt{s_{\mathrm{NN}}} = 5.02$ TeV, Eur. Phys. J. C **76**, 245 (2016).
[79] B. Abele *et al.* (ALICE Collaboration), Centrality dependence of π, K and p production in Pb-Pb collisions at $\sqrt{s_{\mathrm{NN}}} = 2.76$ TeV, Phys. Rev. C **88**, 044910 (2013).
[80] B. Abele *et al.* (ALICE Collaboration), K_S^0 and Λ Production in Pb-Pb collisions at $\sqrt{s_{\mathrm{NN}}} = 2.76$ TeV, Phys. Rev. Lett. **111**, 222301 (2013).
[81] B. Abele *et al.* (ALICE Collaboration), Multi-strange baryon production at mid-rapidity in Pb-Pb collisions at $\sqrt{s_{\mathrm{NN}}} = 2.76$ TeV, Phys. Lett. B **728**, 216 (2014).
[82] B. Abele *et al.* (ALICE Collaboration), $K^*(892)^0$ and $\phi(1020)$ production in Pb-Pb collisions at $\sqrt{s_{\mathrm{NN}}} = 2.76$ TeV, Phys. Rev. C **91**, 024609 (2015).
[83] S. Acharya *et al.* (ALICE Collaboration), Production of charged pions, kaons, and (anti-)protons in Pb-Pb and inelastic pp collisions at $\sqrt{s_{\mathrm{NN}}} = 5.02$ TeV, Phys. Rev. C **101**, 044907 (2020).
[84] S. Acharya *et al.* (ALICE Collaboration), Production of $K^*(892)^0$ and $\phi(1020)$ in pp and Pb-Pb collisions at $\sqrt{s_{\mathrm{NN}}} = 5.02$ TeV, Phys. Rev. C **106**, 034907 (2022).
[85] S. Acharya *et al.* (ALICE Collaboration), Production of pions, kaons, (anti-)protons and mesons in Xe-Xe collisions at $\sqrt{s_{\mathrm{NN}}} = 5.44$ TeV, Eur. Phys. J. C **81**, 584 (2021).
[86] F. Becattini, J. Cleymans, A. Keränen, E. Suhonen, and K. Redlich, Features of particle multiplicities and strangeness production in central heavy ion collisions between 1.7A and 158A GeV/c, Phys. Rev. C **64**, 024901 (2001).
[87] A. Andronic, P. Braun-Munzinger, K. Redlich, and J. Stachel, Decoding the phase structure of QCD via particle production at high energy, Nature (London) **561**, 321 (2018).
[88] F. A. Flor, G. Olinger, and R. Bellwied, Flavour and energy dependence of chemical freeze-out temperatures in relativistic heavy ion collisions from RHIC-BES to LHC energies, Phys. Lett. B **814**, 136098 (2021).
[89] F. A. Flor, G. Olinger, and R. Bellwied, System size and flavour dependence of chemical freeze-out temperatures in ALICE data from pp, pPb and PbPb collisions at LHC energies, Phys. Lett. B **834**, 137473 (2022).
[90] L. Adamczyk *et al.* (STAR Collaboration), Strange hadron production in Au+Au collisions at $\sqrt{s_{\mathrm{NN}}}$ =7.7, 11.5, 19.6, 27, and 39 GeV, Phys. Rev. C **102**, 034909 (2020).
[91] B. I. Abelev *et al.* (STAR Collaboration), Systematic measurements of identified particle spectra in pp, d+Au, and Au+Au collisions at the STAR detector, Phys. Rev. C **79**, 034909 (2009).
[92] G. Agakishiev *et al.* (STAR Collaboration), Strangeness Enhancement in Cu-Cu and Au-Au Collisions at $\sqrt{s_{\mathrm{NN}}} = 200$ GeV, Phys. Rev. Lett. **108**, 072301 (2012).
[93] C. Tsallis, *Introduction to Nonextensive Statistical Mechanics* (Springer, New York, 2009).